PREDICTING CONSTRAINT POINT LOADS FOR A VEHICLE TOWED ALONG A FIXED PATH

By

JARROD BRAUN

Bachelor of Science in Mechanical Engineering

University of Tulsa

Tulsa, Oklahoma

2018

Submitted to the Faculty of the
Graduate College of the
Oklahoma State University
in partial fulfillment of
the requirements for
the Degree of
MASTER OF SCIENCE
December, 2020

PREDICTING CONSTRAINT POINT LOADS

FOR A VEHICLE TOWED ALONG A

FIXED PATH

Thesis Approved:

Dr. Jerome Hausselle

Thesis Adviser

Dr. Shuodao Wang

Dr. Aurelie Azoug

Name: JARROD BRAUN

Date of Degree: DECEMBER, 2020

Title of Study: PREDICTING CONSTRAINT POINT LOADS FOR A VEHICLE TOWED ALONG A FIXED PATH

Major Field: MECHANICAL AND AEROSPACE ENGINEERING

Abstract: Towing a vehicle along a fixed path is useful in automation processes. Understanding the forces involved while towing a vehicle is critical for the design of the towing system. For aircraft in particular, careful measures must be taken to ensure that loads remain within the envelope prescribed by the manufacturer. These loads may be determined via testing. However, this is expensive, and each vehicle or vehicle configuration requires its own test. An analytical method for predicting loads is much quicker, more cost effective, and more easily enables vehicle compatibility with the system. To create such a method, known models for predicting a vehicle's wheel trajectory are combined with a prescribed velocity profile along the trajectory. From these, the vehicle's linear and angular accelerations at every point along the path are derived. The equations of motion for the vehicle may then be solved to determine key unknown forces, such as the overall towing force and lateral wheel friction. A first validation of this approach was performed by comparing the predicted direction of the lateral towing force to the direction recorded while towing a scale aircraft. The experiment was repeated at multiple speeds. The predicted force direction matched the measured direction for over 94% of the path length at all speeds tested. The highest correlation for any test was 99%, while the lowest was 94.3%. The agreement between the predicted and recorded direction suggest that further investigation of this approach is warranted.

TABLE OF CONTENTS

LIST OF TABLES

Table Page

LIST OF FIGURES

Figure Page

CHAPTER I

INTRODUCTION

This thesis presents an analytical method of predicting the magnitude and direction of forces at the tow-point of a single-axle, two-wheeled vehicle being towed along a fixed path. The approach developed is accurate for a towing link that allows for rotation about the axis perpendicular to the plane of travel. The motivation for this research comes from a new method of transporting aircraft around an airport being developed by Aircraft Towing System (ATS) [6]. ATS is designing a system in which the nose gear of an aircraft is attached to a cart that travels along an in-ground channel (Figure 1). The system operates without the need for the many crewmen who coordinate many pilots taxiing at an airport.

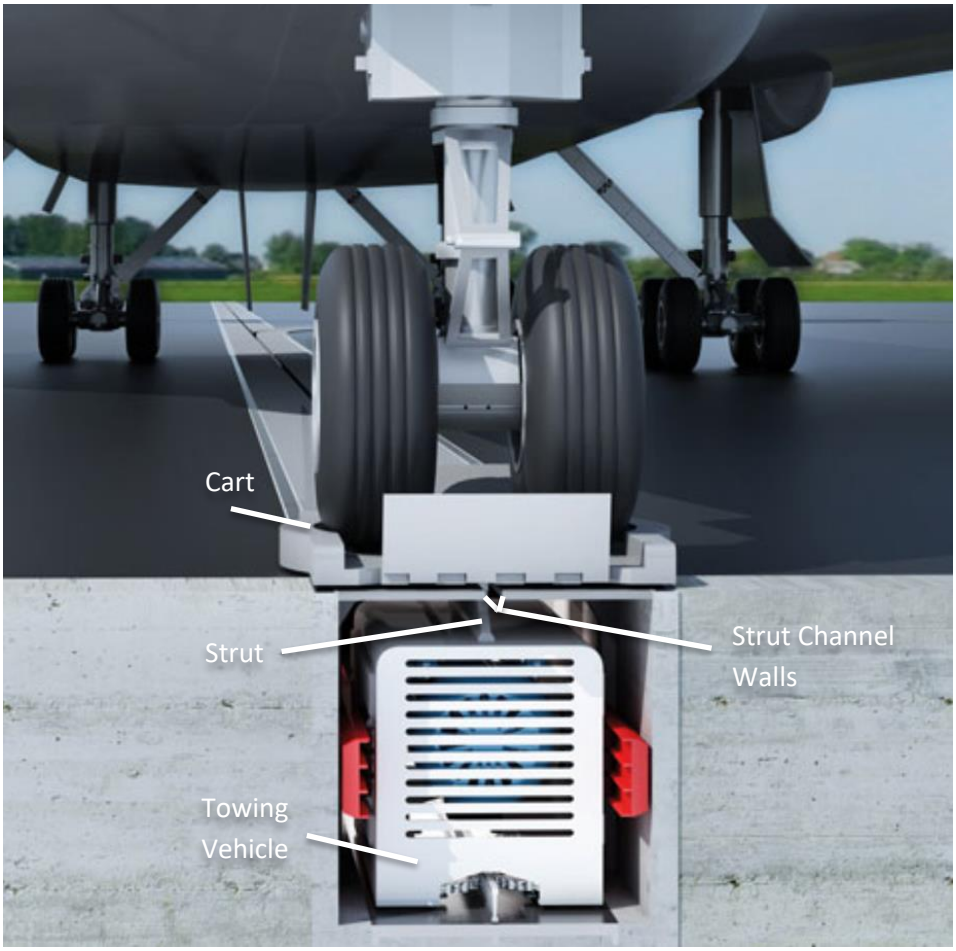

Figure 1: General Layout of ATS System [6]

It is critical to understand the forces at the tow-point for both the design of the towing system and the loading of the aircraft. The designer must understand the forces involved in order to determine the overall design configuration as well as specific dimensions and material selections. For example, a high magnitude of the load may necessitate a strut with wheels on the side to roll against the channel wall. A low force magnitude could allow for a sliding friction design. Should a simple friction design be chosen, the magnitude of friction must be known in order to select an adequately powered towing system. Structurally, the designer must consider both static failure and failure by fatigue, which requires accurate prediction of both the magnitude and direction of the forces at the tow-point. Failure of the towing system could be potentially catastrophic, ending

with a runaway aircraft. Damaged to the towed aircraft and potentially other aircrafts would cost millions in repair costs and revenue losses due to being ground. At worst, it could injure or kill human workers on the airport grounds.

Additionally, the designer must ensure that loads fall within acceptable nose gear loads and load cycles as prescribed by the aircraft manufacturer. Aircraft maintenance, inspection, and repair cycles are designed around specific load spectra. Therefore, any loads placed on the nose gear by ATS must fall within those parameters. If they do not, damage to the aircraft such as cracking could occur before the normal inspection time. This could lead to failure of the nose gear should the cracking be bad enough.

One of the goals in predicting the forces at the tow-point is understanding what parameters most significantly affect those forces, which will drive design decisions and operating parameters. For example, the mass of the aircraft, its rotational inertia, friction along the channel wall, wind load, velocity at tow-point, and path layout all affect the load magnitude and overall load spectrum. These parameters may need to be bounded in order to keep the load within the aircraft manufacturer's prescribed envelope or to allow for a sufficiently small strut.

The high-level steps of predictive method described in this paper are described briefly below.

1. Obtain discretized trajectory of MLG for predefined nose gear trajectory
2. Assign speed to at each point of trajectory
3. Differentiate discretely to obtain velocities and accelerations
4. Use the calculated accelerations and other known forces to solve for unknown forces, such as forces on the strut

Although the primary application discussed in this paper is for towing aircraft, the core philosophy may be applied to other towed vehicles such as trailers or tractor attachments, but also anything attached to a single tow-point that allows for rotation about the vertical axis.

CHAPTER II

REVIEW OF LITERATURE

Current literature does not sufficiently address the requirements for a fully analytical model for a system like ATS due to its unique kinematic properties and model requirements. These are the following:

- Nose gear follows predefined path
- Presence of a pulling force at the nose gear
- Forces must be known at every point along the trajectory
- Model must be applicable to variety of aircraft

MLG trajectory prediction models exist, but they are formed as a response to steering input on the nose gear [1][2]. The problem with this approach is that the nose gear trajectory is also determined by the steering inputs. Since a predefined path will be defined for the ATS system rather than a series of steering inputs, these methods need to be adapted to be useful. Rejendran et al have done just this [3]. They calculate steering inputs at each path point necessary for the nose gear to follow the predefined trajectory. Then, these steering inputs may be used to calculate the trajectory of the MLG.

Methods also exist to determine the lateral forces on the nose gear and MLG during a typical taxiing situation [4]. The techniques used in this method are applicable to the ATS system, however it falls short in two ways. The first is that it does not feature the presence of a pulling force on the nose gear. The second is that it assumes constant speed, neglecting accelerations caused by thrusting or braking. Obviously, aircraft in the ATS system need to accelerate to towing speed, so the force calculation method presented by You et al is insufficient.

Khapane has combined trajectory prediction and lateral force calculation to predict landing gear lateral forces at every point along the trajectory [5]. This investigation also takes into account accelerations caused by braking. However, the nose gear pulling force present in the ATS system is not modeled.

This paper addresses the two major shortcomings of current literature in addressing the requirements of an analytical model for forces present in the ATS system. These shortcomings are the lack of modeling of the pulling force and not incorporating a velocity and acceleration profile to determine forces for a predetermined nose gear path.

CHAPTER III

METHODOLOGY

There are several methods that could be employed to solve this problem. The first most direct method would rely on experimental testing. Forces could be directly measured across a variety of speeds, and a profile could be built for a particular aircraft. The major problem with this approach is that the ATS system is designed to handle a variety of aircrafts. Full-scale testing is simply very impractical and expensive. Additionally, these aircraft would be operating on a new system that has not been validated and proven safe, which could damage the aircraft.

Reduced scale testing carries many of the same problems. Many test scenarios would have to be run in order to build up an accurate profile across a range of aircrafts, which is time consuming. Furthermore, the scale results would have to be correlated to the full-scale aircraft. While this could be done, the effort involved is simply impractical.

An analytical approach eliminates pretty much all of these issues. Computational simulations usually take far less time than physical tests. A multitude of test conditions can be run in parallel in a matter of days, whereas physical tests may take months and even years. Additionally, there is no risk of damage to an actual aircraft. Therefore, an analytical approach was selected to determine the forces at the tow point.

A top-down approach will be taken to convey the method used to determine the tow Point forces. For a body of constant mass, the following must be true:

$$ma = \sum F \tag{1}$$

$$I\alpha = \sum T \tag{2}$$

In the case of an aircraft being towed on a fixed path, many forces are known. A free body diagram of a rolling aircraft being towed along a curved path is shown below in Figure 2.

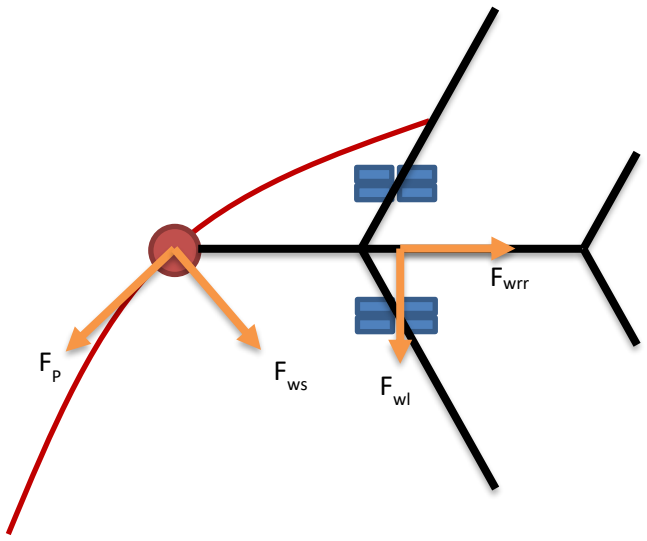

Figure 2: Free Body Diagram of a Rolling Vehicle Traveling Along a Curved Path

A pull force ($\mathbf{F_p}$) acts in the direction tangent to the path. The channel wall exerts a contact force ($\mathbf{F_{ws}}$) on the strut, perpendicular to the tangent line of the path. The tires have a rolling resistance ($\mathbf{F_{wrr}}$) opposite the direction of motion of the MLG. Additionally, a lateral frictional force ($\mathbf{F_{wl}}$) exists at the main landing gear wheels that prevents the tires from skidding laterally. Therefore, taking moments about the center of mass in the X,Y plane , equations 1 and 2 become:

$$m\boldsymbol{a_{cg}} = \boldsymbol{F_{wrr}} + \boldsymbol{F_{wl}} + \boldsymbol{F_{ws}} + \boldsymbol{F_p} \tag{3}$$

$$I\boldsymbol{\alpha} = \boldsymbol{R_{wl}}\, x\, \boldsymbol{F_{wl}} + \boldsymbol{R_{ws}}\, x\, \boldsymbol{F_{ws}} + \boldsymbol{R_p}\, x\, \boldsymbol{F_p} \tag{4}$$

However, it is beneficial to expand Equations 3 and 4 slightly further:

$$m\boldsymbol{a_{cg}} = F_{wrr}\boldsymbol{u_{wrr}} + F_{wl}\boldsymbol{u_{wl}} + F_{ws}\boldsymbol{u_{ws}} + F_p\boldsymbol{u_p} \tag{5}$$

$$I\boldsymbol{\alpha_{cg}} = \boldsymbol{R_{wl}}\, x\, F_{wl}\boldsymbol{u_{wl}} + \boldsymbol{R_{ws}}\, x\, F_{ws}\boldsymbol{u_{ws}} + \boldsymbol{R_p}\, x\, F_p\boldsymbol{u_p} \tag{6}$$

This final form presented in Equations 5 and 6 is useful because several of these parameters are known. The mass and rotational inertia of an aircraft may be estimated. the direction of the pull Force ($\boldsymbol{u_p}$), channel wall force on the strut ($\boldsymbol{u_{ws}}$), MLG rolling resistance ($\boldsymbol{u_{wrr}}$), and wheel lateral friction ($\boldsymbol{u_{wl}}$) are all known at every point along the path. However, it must be noted that the pull force and channel force on strut could be reversed depending on the motion of the aircraft. In this case the value of the magnitude of the force would simply be negative. Equations also exist to determine the rolling resistance of pneumatic tires, allowing F_{wrr} to be calculated. This leaves the following five parameters to be determined:

1. Magnitude of pull Force (F_p)
2. Magnitude of Channel force on nose gear (F_{ws})
3. Magnitude of the wheel lateral friction (F_{wl})
4. Linear acceleration of the center of mass of the aircraft ($\boldsymbol{a_{cg}}$)
5. Angular acceleration about the center of mass of the aircraft ($\boldsymbol{\alpha_{cg}}$)

If the linear and angular accelerations can be determined, a system of three equations with three unknowns remains, with the unknown parameters being the magnitude of the pull force (F_p), magnitude of the channel force on the nose gear (F_{ws}), and wheel lateral friction (F_{wl}).

The bulk of the effort of this method comes from determining the linear and angular accelerations. If the linear velocity of the CG is known, it can be differentiated to obtain the linear acceleration. The method used to obtain the velocity of the CG is as follows.

First, the trajectory of the CG as the aircraft is towed along the path is determined. Previous work laid out an analytical method for predicting the trajectory of a towed aircraft with the same constraints present in the ATS system [3]. In this approach, the trajectory is determined geometrically. That is to say, given certain angles taken from the geometry of the aircraft and nose gear path, and given the next location of the nose gear, the location of the main landing gear at the next point is calculated. The trajectory of the landing gear is thus discretized across the entire nose gear path. Since the position of at least two points on the aircraft are known at every step along the path, the position of any other point on the aircraft can be calculated at any step along the path, which leads to the determination of the trajectory of the CG.

Following position calculation, the velocity of the CG is calculated. If the time it takes the CG to travel from one discretized point to the next is known, velocity becomes an easy calculation. This time may be determined by assigning a velocity to the nose gear at every point along the path, with the direction parallel to the tangent line of the path and in the direction of travel. This assignment is reasonable because in a system such as ATS, velocity at the path is likely to be controlled by some predetermined speed profile. For example, the control system may be programmed to increase the speed of the cart to 5mph, hold that speed for a certain distance, then decelerate to a stop. The time taken for any positional step is the same for all points on the

aircraft, including the CG. Therefore, it becomes straightforward to calculate the velocity of the CG at all points along the path via discrete differentiation.

$$\boldsymbol{v_n} = \frac{\boldsymbol{R_n} - \boldsymbol{R_{n-1}}}{\Delta t} \tag{7}$$

With velocities and time for each step known, a second discrete differentiation yields linear acceleration.

$$\boldsymbol{a_n} = \frac{\boldsymbol{v_n} - \boldsymbol{v_{n-1}}}{\Delta t} \tag{8}$$

Angular acceleration is similarly calculated. The vector pointing from the CG to the nose gear, as well as its angular position, θ, is known at every step of the trajectory. Since the aircraft is considered a rigid body, the angular acceleration of this vector is the angular acceleration of the entire body about the CG. Consequently, this angular acceleration may be used in the torque balance shown in Equation 6. Differentiating θ once yields angular velocity about the CG.

$$\omega_n = \frac{\theta_n - \theta_{n-1}}{\Delta t} \tag{9}$$

A second differentiation produces angular acceleration.

$$\alpha_n = \frac{\omega_n - \omega_{n-1}}{\Delta t} \tag{10}$$

At this point, the system of equations given by Equations 5 and 6 may be solved for the remaining three unknowns: F_{ws}, F_{wl}, and F_p. Sample simulation output is shown in Figure 4 for a 787-8 being towed on the path shown in Figure 3.

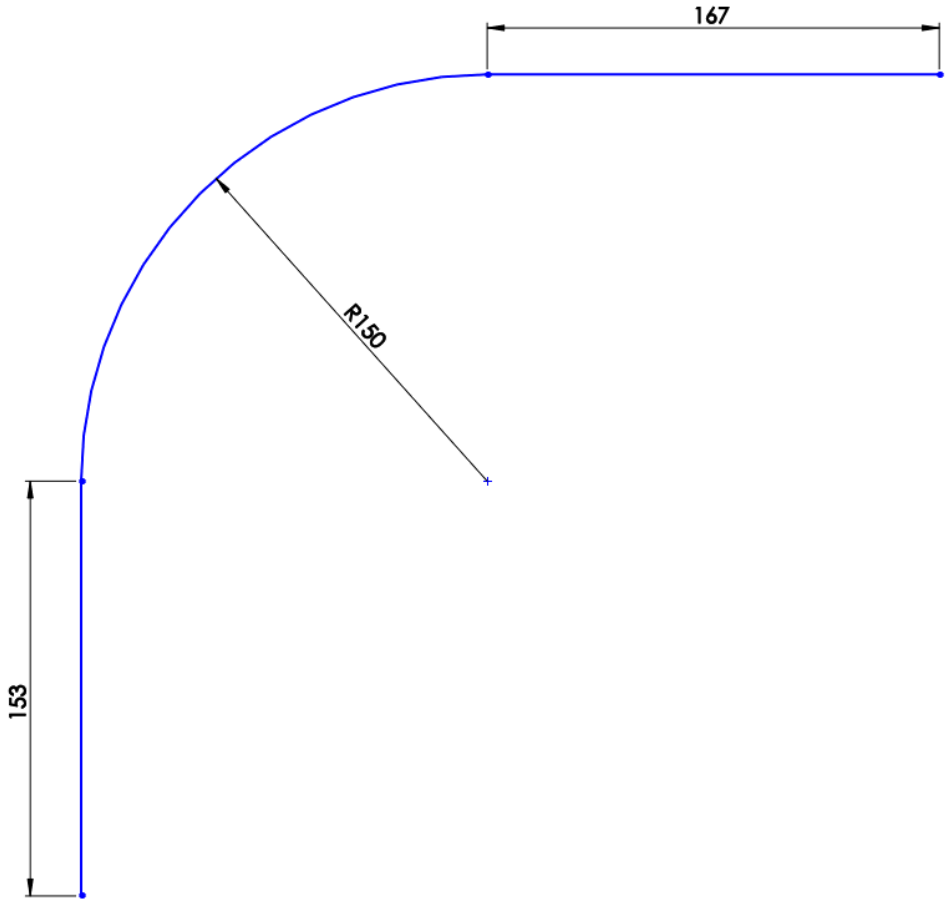

Figure 3: Sample Path for 787-8 (Dimensions in Feet)

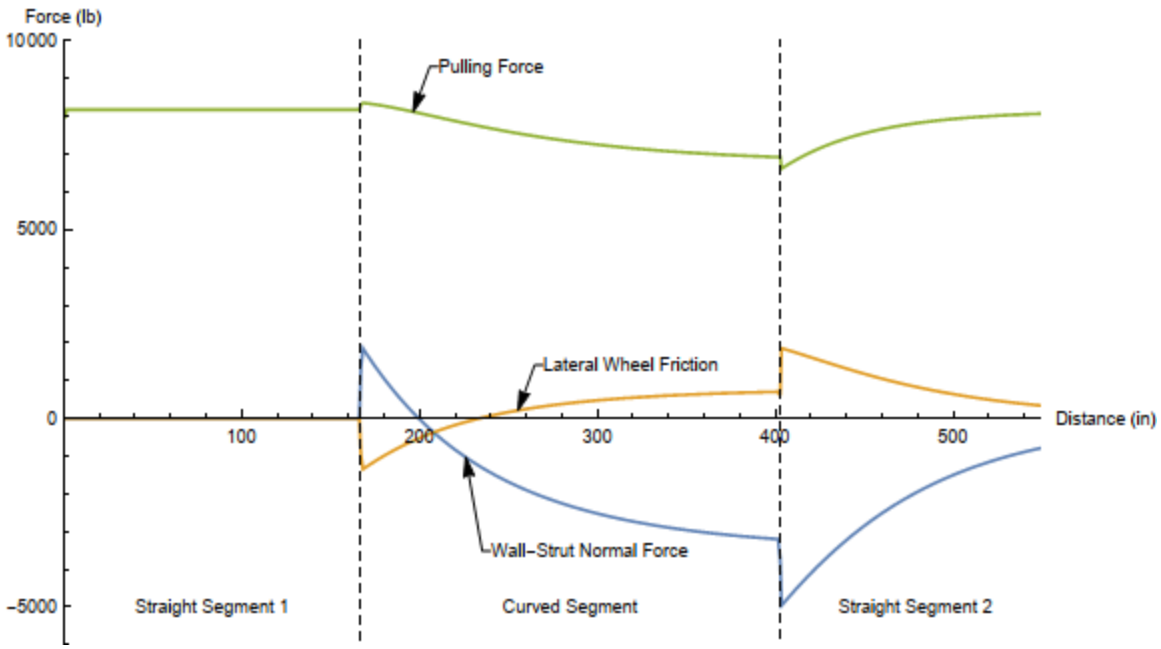

Figure 4: Simulation Output for 787-8 Towed Along Sample Path

An important thing to note is that as a discrete prediction method, there is a certain step size at which the solution converges. Clearly, the convergence step size varies depending on the aircraft's wheelbase. That is to say, an error of one foot is a much more significant trajectory deviation for an aircraft with a ten-foot wheelbase than it is for an aircraft with an eighty-foot wheelbase. For this reason, convergence step size was evaluated as a percentage of the wheelbase.

Since the forces predicted by the simulation rely primarily on the speed profile and path step size prescribed to the cart path, solution convergence is reached when cart acceleration convergence is reached. Acceleration convergence is determined by calculating the average percent deviation from one step size to the next lowest step size. Step sizes were halved so that acceleration points could be compared directly. For example, if a track length of 12 inches was discretized at a step size of 4 inches, there would be 3 possible acceleration points. If the same track was discretized at a 2-inch step size, there would be 6 points, 3 of which are common to the coarser 4 inch

discretization. The average percent deviation between acceleration at these 3 common points is then calculated. As the average percent deviation approaches zero, the acceleration solution for the entire path converges.

Note that step size needs to be halved in order to achieve the most common points. If the 12-inch track from the above examples was discretized from 4 inches first and 3 inches second, there would be 3 acceleration points and 4 acceleration points respectively. None of these points would be shared between both sets because they occur at different distances along the track. It could not be known if the simulation is converging on a solution because accelerations at the same distance along the track could not be compared.

The sample path from Figure 3 above was used to determine step size convergence. Each segment was discretized into a certain number of points, beginning at 25 and doubling until reaching 800. The largest segment step size in feet, percentage of 787-8 wheelbase, and the average percent deviation of accelerations from points common with the previous step size is shown in Table 1 below.

Table 1: Acceleration Convergence (787-8)

No. Points	Step Size (ft)	Step Size (% Wheelbase)	Average % Deviation from Previous
25	6.68	8.94	-----
50	3.34	4.47	1.78
100	1.67	2.23	0.96
200	0.835	1.12	0.50
400	0.418	0.559	0.25
800	0.209	0.279	0.18

As expected, the average percent deviation decreases as step size decreases. Due to computational expense, the solution is assumed to have sufficiently converged when percent deviation reaches 0.50%. This occurs at a step size of 1.12% of the wheelbase (200 points per segment). Therefore, a 1.12% path step size was chosen for all simulations moving forward. Note that the results shown in Table 1 were found to be independent of speed.

CHAPTER IV

VALIDATION

In order to quantify the accuracy of the simulation results, a scale aircraft was towed along an appropriately scaled path. The inputs required for the prediction simulation were recorded and fed into the simulation. As a reminder, those inputs are the following: nose gear speed profile, aircraft mass, aircraft rotational inertia, and the output of the simulation was then compared to the forces measured during the test.

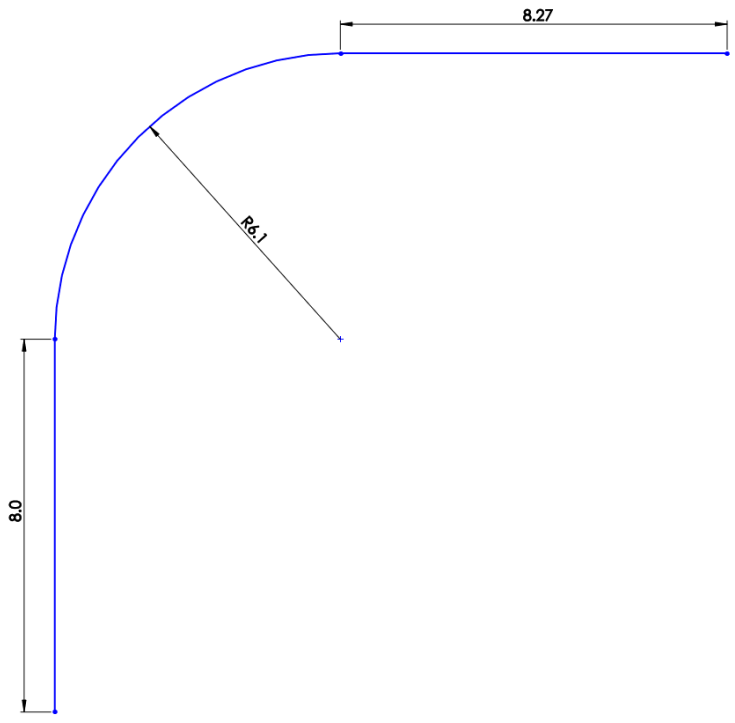

Figure 5: Path Used for Scale Model During Experiment (Dimensions in Inches)

The cart and strut design was mimicked to propel the aircraft along the track. An in-ground channel was not created. Instead, a path was plotted on the ground, and the cart was rolled by hand to follow the path. Note that it was not attempted to follow a predetermined velocity profile when rolling the cart. Rather, the velocity of the cart during a given run was recorded and used as the velocity profile input for the simulation. The strut was allowed to slide slightly inboard or outboard along a short rod. Stops on either end of the rod acted as the channel wall as shown in Figure 6.

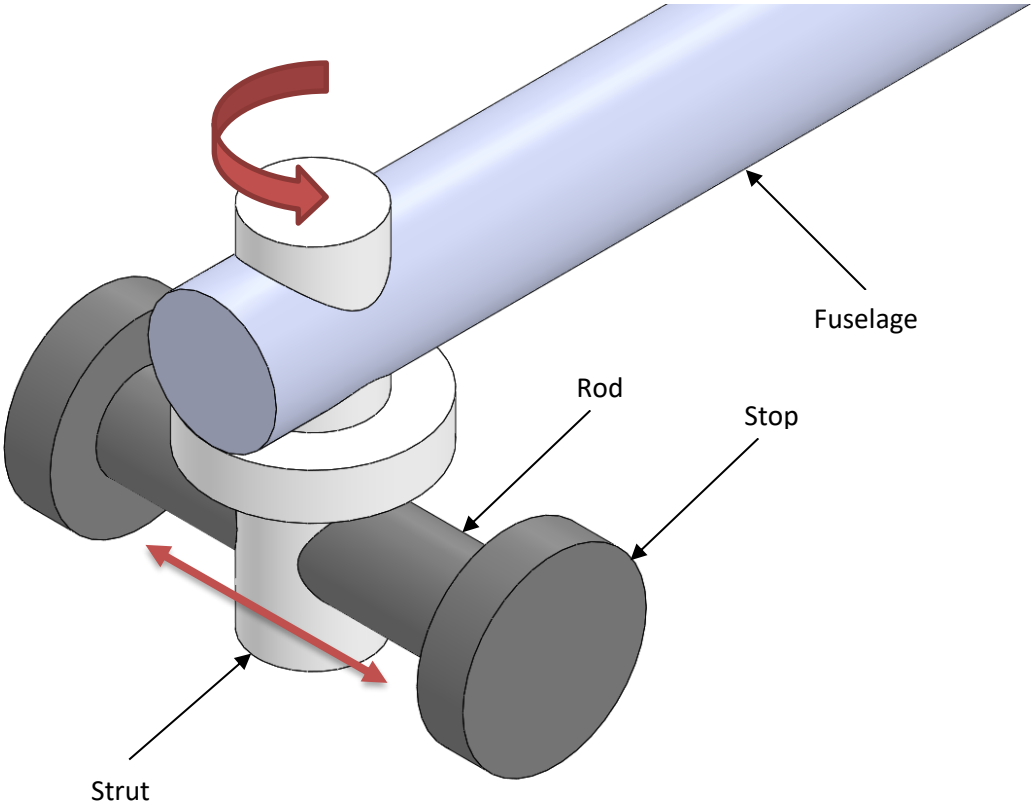

Figure 6: Experiment Tow-Point Layout

Instruments capable of measuring the forces at the tow-point were unable to be obtained, so the magnitudes of the forces were not validated. However, the sign (direction) of the channel force on the strut was recorded. Video was taken of each test, and the tow-point could be visually seen on

either end of the rod as it progressed along the track. This clearly showed whether the channel force was directed inboard or outboard.

An optical encoder was mounted to the axle of the cart. The pulses were used to determine how far along the path the cart had traveled. The time between pulses was used to determine the instantaneous velocity at every pulse point along the path. A challenge involving the speed profile was expanding the recorded speed profile to the discretized path. For acceleration convergence, the required path step size was 0.075 inches. However, the encoder resolution and cart wheel size only allowed for a minimum distance of 0.30 inches per pulse. This meant that there was not a recorded velocity for each discretized point along the path. To remedy this, the constant acceleration required to change the measured velocity over the encoder step size was calculated for every step. With step time, initial velocity, and acceleration known, velocity can be expressed as the following

$$v_n = \sqrt{2a_n(s_n - s_m) + v_m^2} \tag{11}$$

where *n* refers to a discretized path point, and *m* refers to the nearest measured speed point recorded at a distance before s_n.

Following this approach, velocities in between measured encoder positions can be reasonably estimated. The error of these extrapolated velocities cannot be computed directly because the true velocity is not measured. However, it is highly likely that they fall between the measured velocities due to the relatively fine encoder resolution (18 degrees per pulse) and lack of sudden high acceleration while the cart is being rolled. In Figures 7-8 below, the coarse encoder position and corresponding velocity are compared to that data extrapolated to the finer path discretization required for acceleration convergence. Clearly, the extrapolated velocities support the trend set by the measured velocities.

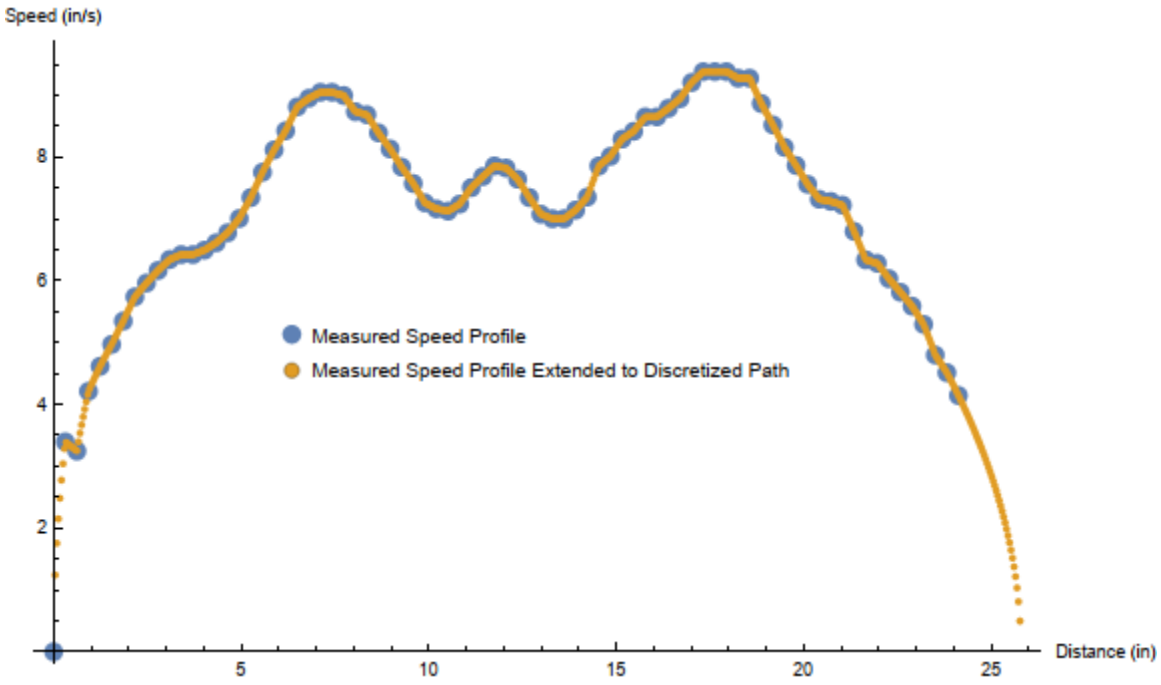

Figure 7: Measured Speed Profile Extended to Finely Discretized Path

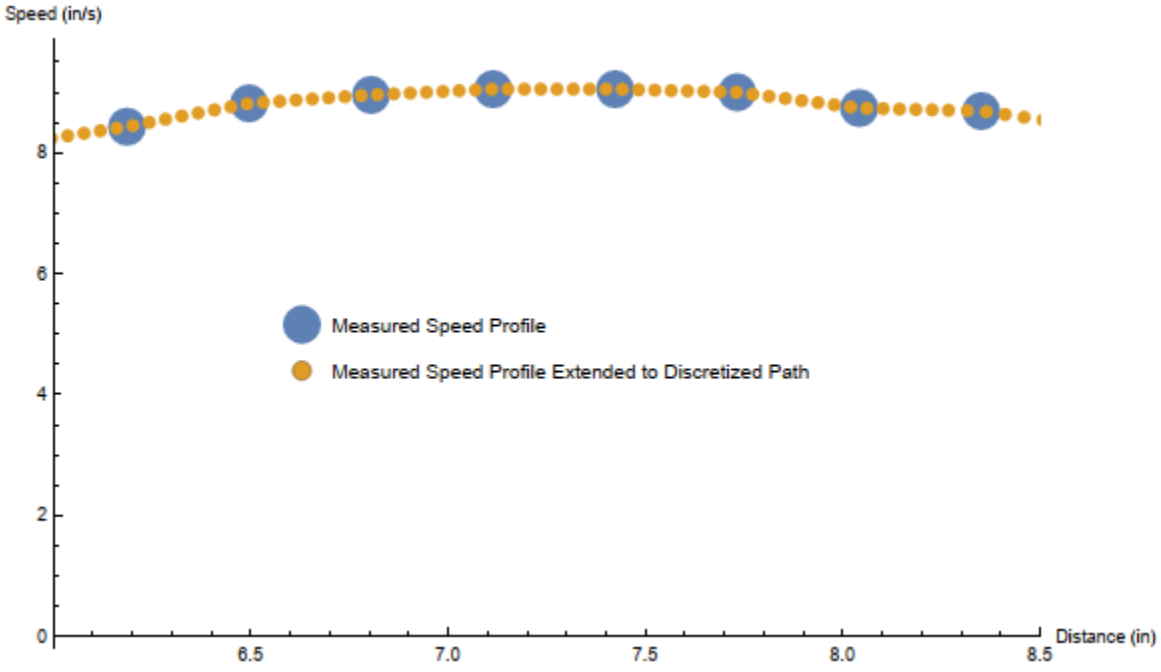

Figure 8: Close Up of Speed Profile Extension

This fitted velocity profile can then be used in the simulation to calculate accelerations.

The physical properties of the scale aircraft (mass, rotational inertia, and CG) were obtained by modeling it in a CAD software.

In order to measure the accuracy of the simulation in predicting the wall-strut force, test points that include both positive and negative force signs must be determined. A correct prediction of the sign for a range of conditions would provide a first validation of the computational model. There are several parameters that affect the wall-strut force: aircraft rotational inertia, mass, MLG rolling resistance, and cart speed. Of these, MLG rolling resistance is unlikely to change. However, the others are highly variable. Mass is dependent on flight occupancy, luggage weight, and fuel conditions. Consequently, rotational inertia will vary greatly since fuel is often stored in the wings of an aircraft. Currently, the final cart speed for a system like ATS is unknown, so it is considered as a parameter for the simulations. Furthermore, the cart speed could be different depending on the location of the aircraft at the airport. As predicted by the simulation, the wall-strut force's sensitivity to changes in rotational inertia, mass, and cart speed are depicted below in Figures 9-11. Note that "nominal" indicates the actual value of the parameter for the test model aircraft. Unless otherwise indicated, rotational inertia and mass values are nominal, and cart speed is 12 in/s.

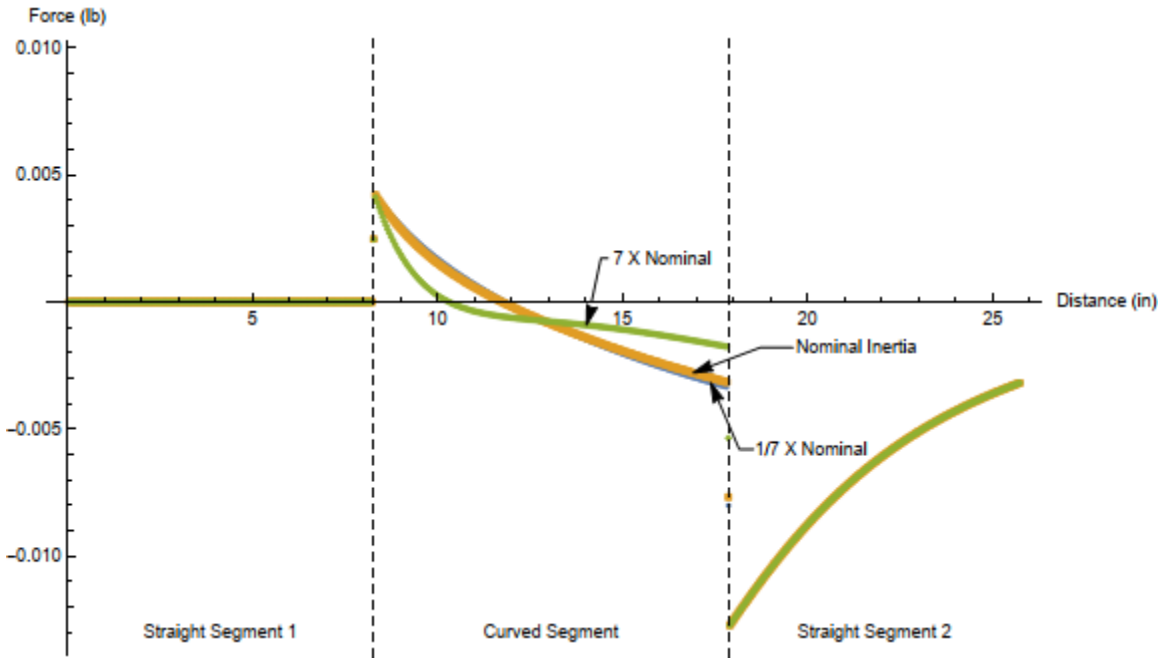

Figure 9: Wall-Strut Force Sensitivity to Rotational Inertia

In Figure 9 above, the simulation shows the relationship between rotational inertia and wall-strut force to be quite weak. At just 1/7th of the nominal value the force is nearly identical over the entire path. At 7 times the nominal value, the force profile does change a bit, but only during the curved section of the path. Given the small difference in force profile despite such a large range of rotational inertia values, rotational inertia was not varied during the experiment.

There is a much greater sensitivity to mass, as shown in Figure 10, than to any other parameter considered. The wall-strut force value translates to almost completely negative to completely positive along the curved segment at only 50% deviation from nominal mass. This heightened sensitivity can be explained by Newton's third law and the free body diagram presented earlier.

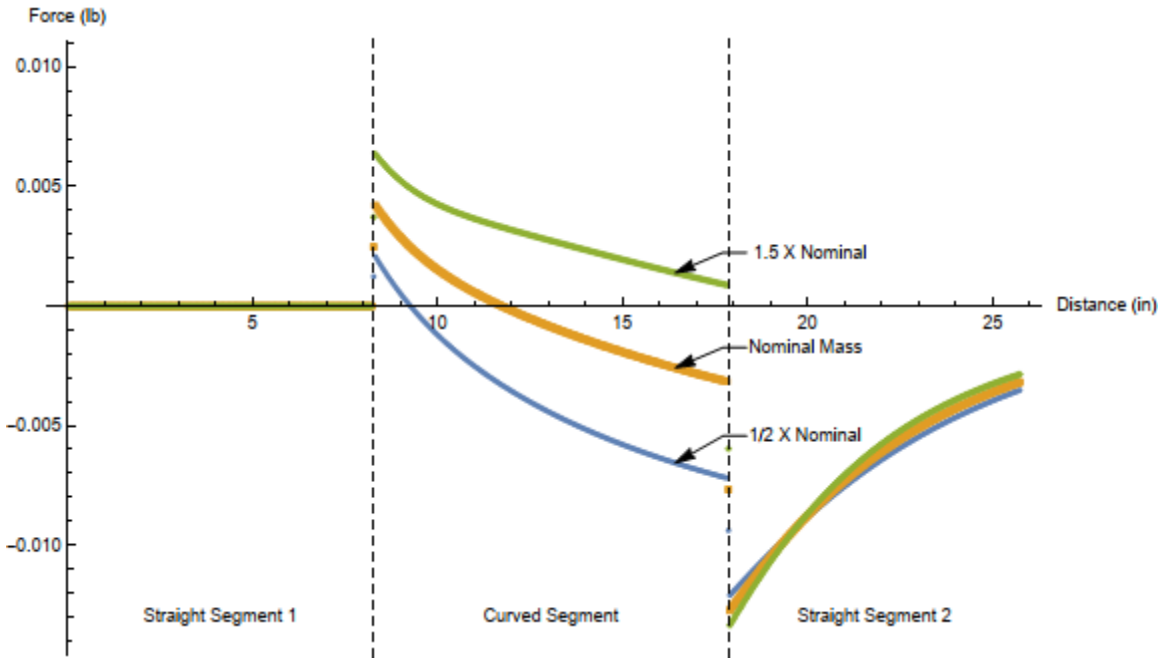

Figure 10: Wall-Strut Force Sensitivity to Mass

No matter what, the acceleration of the CG of the aircraft must be what is derived from the path prediction and speed profile. This is because the aircraft path is independent of everything except landing gear configuration, and the speed profile is prescribed arbitrarily. Now, the only constant force is the MLG rolling resistance. When the aircraft mass is relatively small, the rolling resistance causes a greater acceleration opposite the path direction and into the interior channel wall. As mass increases, the acceleration due to rolling resistance decreases. However, the overall required acceleration remains the same as dictated by the aircraft path and speed profile. In order to make up for this acceleration deficit the other forces increase accordingly, including the wall-strut force.

Although altering the mass does create a measurable variation in wall-strut force, this proved to be impractical during experimentation. In order to change mass without also changing rotational inertia about the CG, additional mass could only be located at the CG. This was possible, but the added mass also raised the vertical CG coordinate. This led to tipping problems when traveling

around the curved portion of the path. For this reason, mass was eliminated as a test point parameter.

Cart speed variation produced a very similar wall-strut force response as mass. This is shown below in Figure 11.

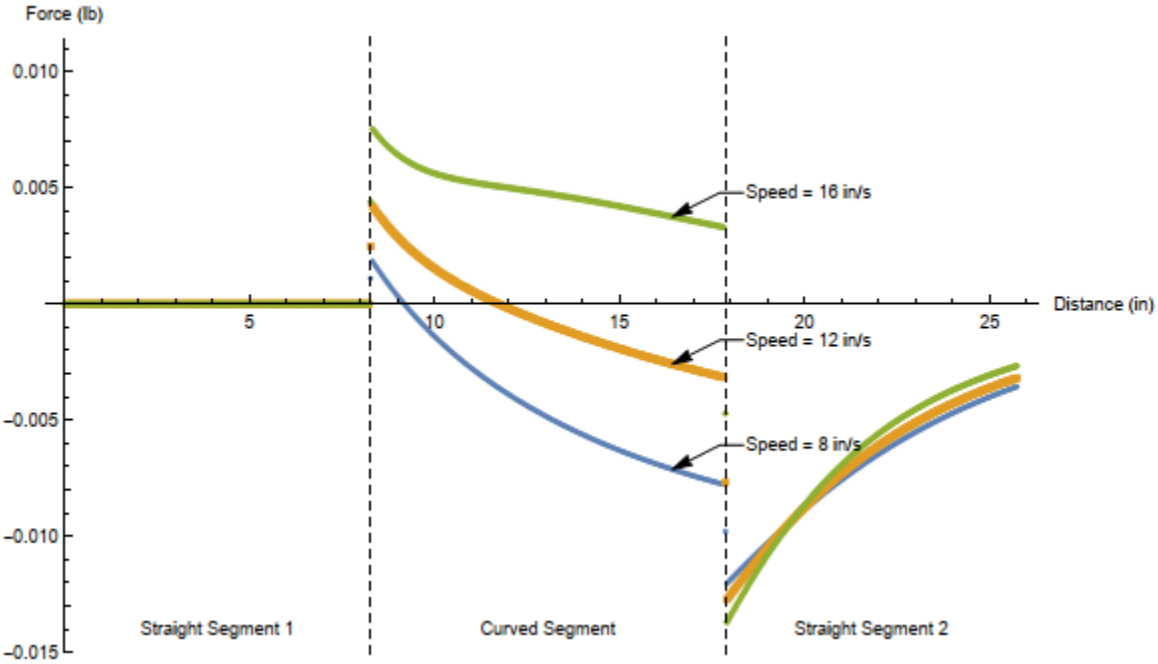

Figure 11: Wall-Strut Force Sensitivity to Cart Speed

The explanation for why the sensitivity is so great is also very similar to that for mass. Higher speed causes higher acceleration around the curve, particularly centripetal acceleration. MLG rolling resistance remains the same and can therefore only cause an unchanging acceleration. So when the required acceleration increases, other forces must increase, thereby creating the higher acceleration of the aircraft. The reason it affects the wall-strut force so much is explained by the free body diagram. Recall that a positive wall-strut force acts toward the center point of the quarter circle while along the curved segment. This is approximately the direction of the centripetal acceleration of the CG of the aircraft (but not exactly the same direction because the CG follows a slightly different trajectory than the cart, but still curved). When centripetal

acceleration increases, the centripetal force must also increase. The wall-strut force is the dominant centripetal force.

Speed is clearly the most easily manipulated parameter during experimentation. One must simply roll the cart faster or slower. This, combined with its large effect on wall-strut force value, is why speed was chosen as the independent variable for the experiment.

The cart was qualitatively rolled at slow, medium, and fast speeds and verified to be at sufficiently different speeds during data processing. The experiment was repeated multiple times to ensure adequate speed separation between runs. Table 2 shows the average cart speed for each run.

Table 2: Average Cart Speed per Run

Run	**Average Cart Speed (in/s)**
Slow	2.2
Medium	6.0
Fast	18.0

CHAPTER V

RESULTS AND DISCUSSION

The simulation's predicted wall-strut force matches very well with the sign measured during the experiment. The results for each speed are discussed on the following pages.

The slow speed run results are shown below in Figure 12.

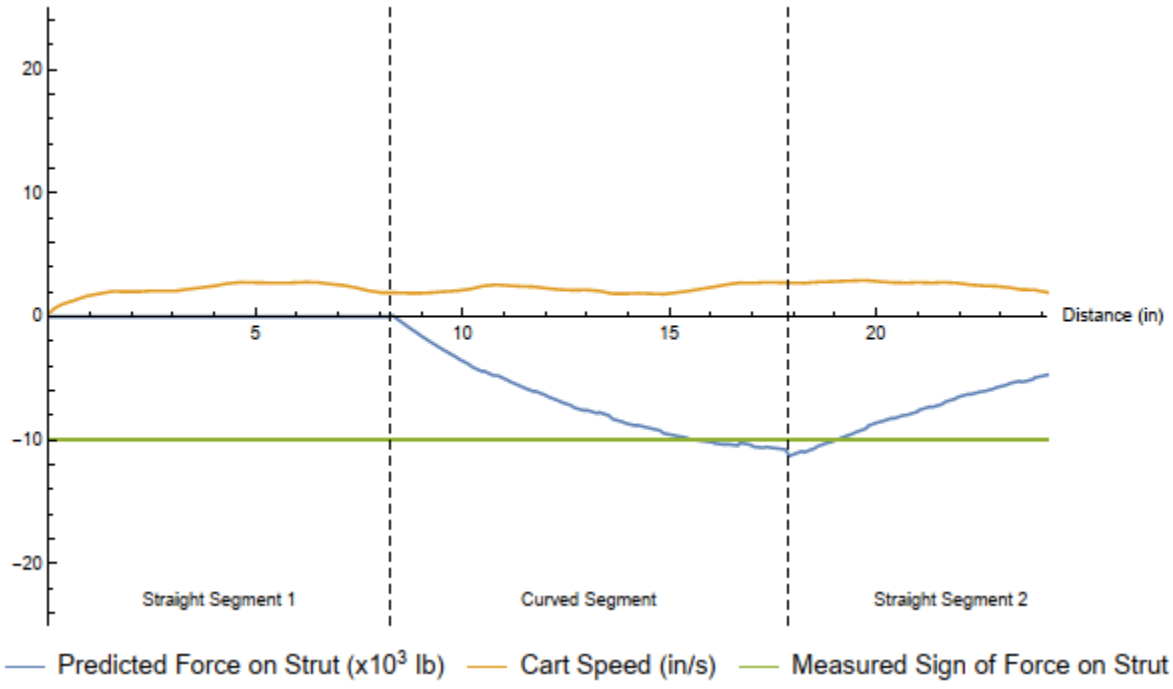

Figure 12: Simulation Output for Slow Speed Run

The average speed for the slow run is 2.2 in/s, and the predicted sign of the wall-strut force is entirely negative. This is consistent with the results of the speed sensitivity examination, in which the sign was nearly always negative at a cart speed of 8 in/s. The measured wall-strut sign is the same as the predicted sign for 99.7% of the path length.

The medium speed at an average of 6.0 in/s yielded similar results, shown below in Figure 13. The measured wall-strut sign is the same as the predicted sign for 95.9% of the path length.

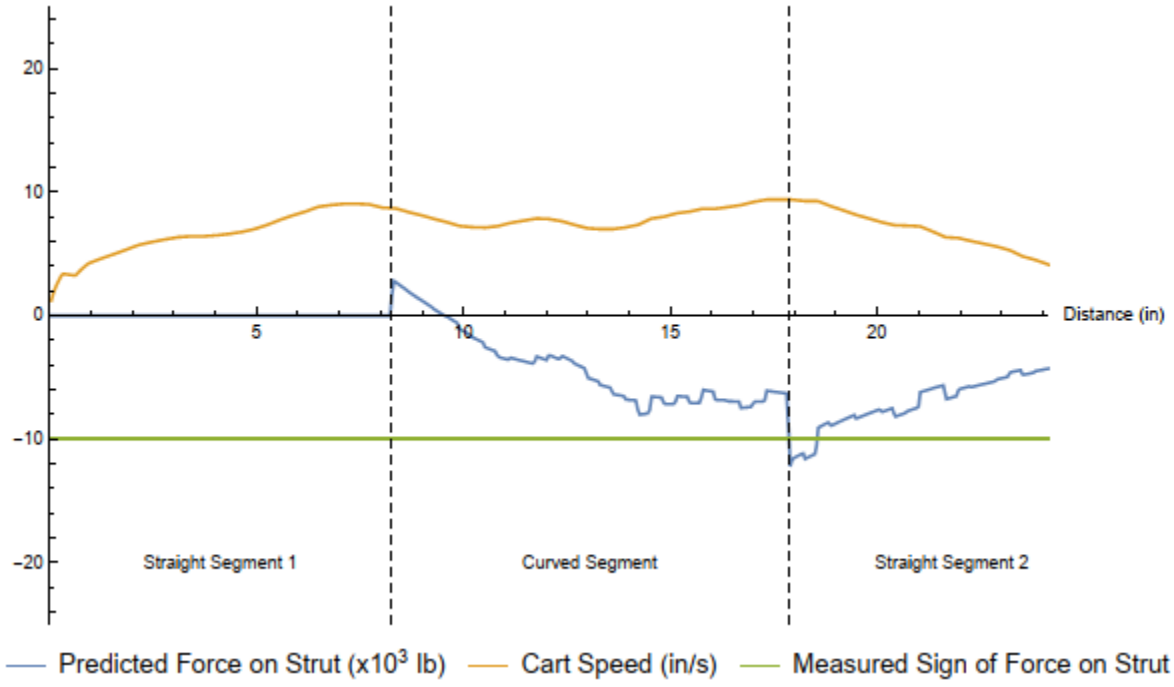

Figure 13: Simulation Output for Medium Speed Run

The small discrepancy at the beginning of the curved segment can be explained by friction. The experimental design is such that the wall-strut force is provided by the stops on the end of the rod. However, some friction exists between the strut and rod. This friction is not accounted for in the simulation. Since the frictional force acts in the same direction as the wall-strut force, a small predicted wall-strut force could be created by friction rather than contact between the stop and strut.

The output of the medium speed run yields another notable result. The local wall-strut amplitude changes that exist over the entire path. This is due to sudden acceleration changes. This is subtle in the medium speed test, but the effect is even more present in the fast run due to the higher speed.

The results of the fast run at 18.0 in/s are shown below in Figure 14. Largely, the simulation output matches what was seen in the experiment at 94.3% correlation.

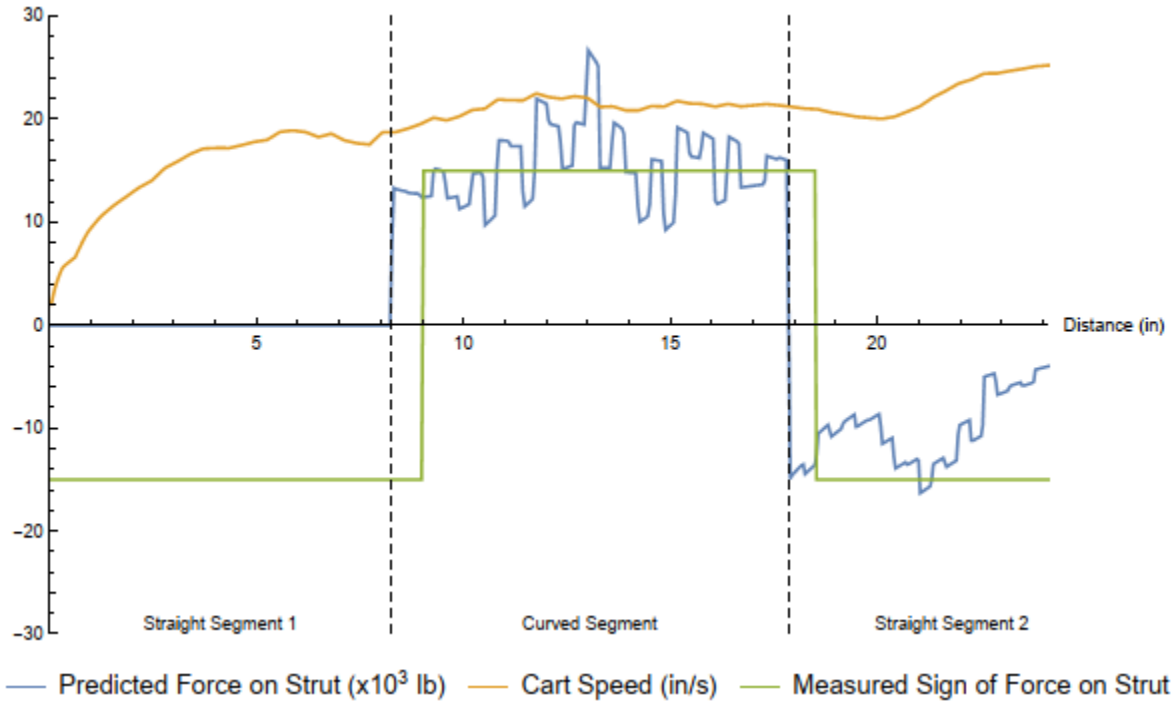

Figure 14: Simulation Output for Fast Speed Run

The cart speed plot is quite noisy, meaning that the measured speed was not smooth and consistent. A likely source of this is wheel slippage on the cart. While performing the tests, axle friction would sometimes cause the cart wheels to lock up momentarily and slide rather than roll. This halted the advancement of the encoder windows, leading to inaccurate speed data. Tests were repeated until no noticeable axle resistance occurred. However, very brief wheel slippage may have gone undetected, leading to the noisy speed data. A zoomed in view of just the curved

section of the fast test run will help make this phenomenon more obvious. This is shown in Figure 15.

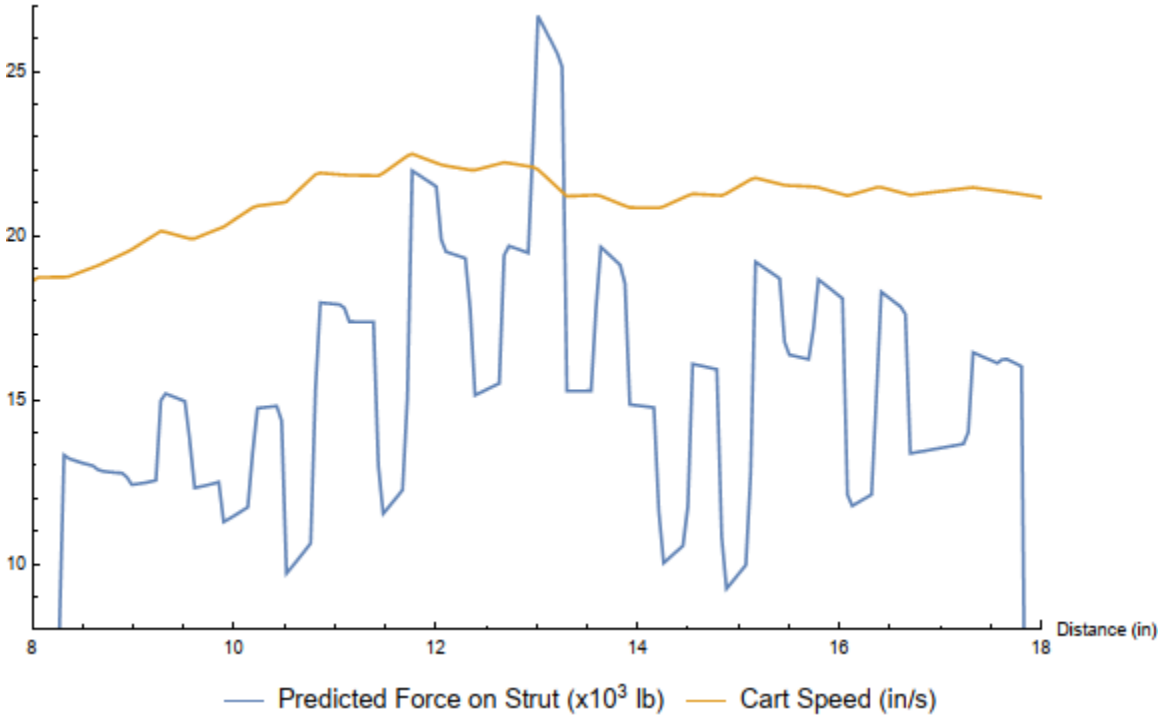

Figure 15: Simulation Output for Fast Speed Run (Close Up View)

As alluded to previously, the amplitude change in wall-strut force present in both the medium and high-speed tests is caused by sudden changes in acceleration. The cart speed appears to be a collection of connected line segments, which is precisely correct. Recall how extra speed data points had to be generated in order to assign a cart speed to every discretized path point. Each line segment is a set of these generated speeds, with the endpoints being actual measured speeds. Nearly all of these measured speed points are inflection points, meaning that the sign of the acceleration changes at these points. Recall that centripetal acceleration is the dominant acceleration when traveling around the curved segment of the path. Since the cart speed does not change drastically from one encoder pulse to the following one, the centripetal acceleration of the aircraft CG from one measured speed point to the next remains mainly constant. However, the

linear acceleration does change significantly from one measured point to the next, so much so that the sign of the acceleration changes. Since total acceleration is a combination of both linear and centripetal accelerations, the total acceleration change is significant. This results in a general wall-strut force trend caused by the centripetal acceleration with both positive and negative deviations from that trend caused by the flip-flopping linear acceleration. This conclusion is especially supported by the region from approximately 8.5 inches to 9.5 inches along the path. In this region the cart's linear acceleration does not change signs and is almost constant throughout the whole segment (based on the slope of the speed plot). The result is a much smoother wall-strut force that follows a very clear trend. This same thing occurs between each measured speed point because the "filler" speeds were generated by assuming constant acceleration. Therefore, for each cart speed segment, the wall-strut force is quite smooth and stable.

In an effort to reduce the noise in the wall-strut force results, alternative differentiation methods for calculating linear acceleration were investigated. The first technique is five point, rather than two point, differentiation. This method retains the amplitude changes produced by two point differentiation, and noise is not significantly reduced. The second technique is fitting a polynomial to the recorded speed data and differentiating the resulting function. This acceleration is then compared to that calculated via discrete differentiation. The continuous acceleration curve differed greatly from the trend exhibited by the discrete acceleration data. Therefore, this smoothing technique is unfit for the data recorded. As a result, velocity differentiation was not altered form the two point method shown previously.

CHAPTER VI

CONCLUSIONS AND RECOMMENDATIONS

Several important conclusions can be made about the simulation and its validation. The first concerns solution convergence and path step size. The force solution converges when acceleration converges, and acceleration convergence is a function of path step size. The path prediction method is dependent on the landing gear geometry. The error at any given step size increases with increasing wheelbase. Wheelbase varies greatly among aircraft. For this reason, step size was examined as a percentage of wheelbase. It was found that a step size of 1.12% of the wheelbase causes the acceleration, and thus the force solution, to converge.

A second conclusion is the sensitivity of the wall-strut force to both aircraft mass and cart velocity. These two parameters have the largest effect on the wall-strut force. This is very important to the design of a system like ATS. Aircraft all have different masses, and even the same aircraft can have a wide mass range depending on number of passengers and current fuel amounts. The mass could drive the allowable velocity profile to ensure loads stay within the operating limits of both the aircraft and the ATS system

Perhaps the most important conclusion is that the experiment was successful in providing a first validation of the analytical method described in this paper. At worst, the measured wall-strut force sign and the sign predicted by the simulation matched for 94.7% of the points recorded for that run. This improved all the way to 99.3% for the slow cart speed run. Although other aspects of the analytical method are not validated, such as the magnitude of the wall-strut force and the magnitudes and signs of the other predicted forces, the strong correlation of the parameter tested suggests that the method as a whole is accurate.

Further experimentation is recommended to validate the analytical method presented in this paper. The experiment conducted in this paper would benefit from a few key improvements. First, results would be more accurate if the cart was constrained to the desired path. In this first validation, the cart was guided by hand along a plotted path. Although the experiment was repeated many times so that the cart followed the path as accurately as possible, there is no doubt it deviated at times. Constraining the cart causes the experiment to more accurately resemble the simulation.

A second validation of the analytical method would be to measure the magnitude of the forces predicted by the simulation. The wall-strut force and pulling force are of particular interest. These are likely the driving factors for the design of a system that can be modeled using this method. Validating these forces would validate the proposed method, especially if a range of vehicle geometries, mass distributions, and cart speeds were tested.

REFERENCES

[1] Franziska Dieke-Meier, Thomas Kalms, Hartmut Fricke, and Michael Schultz Modeling Aircraft Pushback

[2] Erza Hauer, Determination of Wheel Trajectories, 1970, Transportation Journal of ASCE, pp.463-470

[3] Rejendran, Kidd, Fixed Path Pull-In/Push Back Trajectories for Airliner Transport System, 2019, AIAA Aviation 2019 Forum

[4] QingLong You, JingLian Ma & Zhi Zhao Evaluation of the lateral loading caused by aircraft with complex gear configurations turning during taxiing, 2019, International Journal of Pavement Engineering, 20:8, 911-919, DOI: 10.1080/10298436.2017.1366763

[5] Khapane, P. D., Simulation of asymmetric landing and typical ground maneuvers for large transport aircraft, 2003, Aerospace Science and Technology, 7(8), pp. 611-619.

[6] http://www.at-system.eu/system.html

VITA

Jarrod Braun

Candidate for the Degree of

Master of Science

Thesis: PREDICTING CONSTRAINT POINT LOADS FOR A VEHICLE TOWED ALONG A FIXED PATH

Major Field: Mechanical and Aerospace Engineering

Biographical:

Education:

Completed the requirements for the Master of Science in aerospace engineering at Oklahoma State University, Stillwater, Oklahoma in December, 2020.

Completed the requirements for the Bachelor of Science in mechanical engineering at the University of Tulsa, Tulsa, Oklahoma in 2018.

Experience:

Stress Analysist at L3Harris

Aircraft Trajectory Specialist for Aircraft Towing System

Lead Aerodynamics Engineer for University of Tulsa SAE Aero Design Competition team. Achieved second place for technical design presentation among 60 international teams.

Test Engineer for Ameron Pole Products